The crystal structure of coxsackievirus A9: new insights into the uncoating mechanisms of enteroviruses

Elaine Hendry[1†¶], Hideki Hatanaka[1‡¶], Elizabeth Fry[1‡], Michael Smyth[1§], John Tate[1#], Glyn Stanway[2], Juhana Santti[3], Marita Maaronen[3], Timo Hyypiä[3,4] and David Stuart[1,5‡]

Background: Coxsackievirus A9 (CAV9), a human pathogen causing symptoms ranging from common colds to fatal infections of the central nervous system, is an icosahedral single-stranded RNA virus that belongs to the genus *Enterovirus* of the family *Picornaviridae*. One of the four capsid proteins, VP1, includes the arginine-glycine-aspartate (RGD) motif within its C-terminal extension. This region binds to integrin $\alpha_v\beta_3$, the only receptor for CAV9 to be conclusively identified to date.

Results: The crystal structure of CAV9 in complex with the antiviral compound WIN 51711 has been solved to 2.9 Å resolution. The structures of the four capsid proteins, VP1 to VP4, resemble those of other picornaviruses. The antiviral compound is bound in the VP1 hydrophobic pocket, and it is possible that the pocket entrance contains a second WIN 51711 molecule. Continuous electron density for the VP1 N terminus provides a complete picture of the structure close to the fivefold axis. The VP1 C-terminal portion is on the outer surface of the virus and becomes disordered five-residues N-terminal to the RGD motif.

Conclusions: The RGD motif is exposed and flexible in common with other known integrin ligands. Although CAV9 resembles coxsackie B viruses (CBVs), several substitutions in the areas implicated in CBV receptor attachment suggest it may recognise a different receptor. The structure along the fivefold axis provides new information on the uncoating mechanism of enteroviruses. CAV9 might bind a larger natural pocket factor than other picornaviruses, an observation of particular relevance to the design of new antiviral compounds.

Addresses: [1]Laboratory of Molecular Biophysics, South Parks Road, Oxford OX1 3QU, UK, [2]Department of Biological Sciences, University of Essex, Colchester CO4 3SQ, UK, [3]Department of Virology, University of Turku, FIN-20520, Turku, Finland, [4]Haartman Institute, Department of Virology, University of Helsinki, FIN-00014, Helsinki, Finland and [5]Oxford Centre for Molecular Sciences, South Parks Road, Oxford, OX1 3QT, UK.

Present addresses: [†]Centre for Biomolecular Sciences, University of St Andrews, North Haugh, St Andrews KY16 9ST, UK, [‡]Wellcome Trust Centre for Human Genetics, Roosevelt Drive, Oxford OX3 7BN, UK, [§]Department of Biochemistry, University of Leicester, Leicester LE1 7RH, UK and [#]San Diego Supercomputer Center, University of California, San Diego, CA 92093-0537, USA.

[¶]These authors contributed equally to this work.

*Corresponding author.
E-mail: dave@strubi.ox.ac.uk

Key words: picornavirus structure, RGD, uncoating, virus–receptor interaction, WIN compound

Received: 23 July 1999
Revisions requested: 27 August 1999
Revisions received: 5 October 1999
Accepted: 12 October 1999

Published: 30 November 1999

Structure December 1999, 7:1527–1538

0969-2126/99/$ – see front matter

Introduction

Coxsackievirus A9 (CAV9) is a picornavirus of the genus *Enterovirus*. Classification based on pathology and serology has identified 23 coxsackie A virus (CAV) and six coxsackie B virus (CBV) serotypes, however CAV9 is genetically more similar to CBVs and echoviruses than to other CAVs [1]. CAV9 infects humans and is one of the most frequently isolated CAVs, causing a broad range of symptoms from mild cold-like illnesses to fatal infections of the central nervous system [2].

There are six genera in the picornavirus family: the enteroviruses, rhinoviruses, aphthoviruses, cardioviruses, hepatoviruses and parechoviruses. Atomic-resolution structures have been solved for representatives of four out of the six genera [3–6], all of which are broadly similar. The non-enveloped particles are composed of four viral proteins (VPs) that make up a 30nm diameter capsid which surrounds approximately 7500 nucleotides of single-stranded RNA. The capsid possesses icosahedral symmetry, being made up of 60 copies each of the four viral coat proteins VP1 to VP4 which are arranged in T = 1 (pseudo T = 3) symmetry. VP1, VP2 and VP3 each contain in the order of 270 amino acid residues, folded into eight-stranded antiparallel β-sheet structures with a jelly-roll topology, and form the outer surface of the virus.

VP4 contains only about 70 amino acids, and lies on the inside of the capsid. The major differences among the picornavirus structures occur in the surface-exposed loop regions, which define the receptor-binding and principle antigenic sites, and on the inner surface of the virion.

One of the first picornavirus structures to be solved was that of human rhinovirus 14 (HRV14) [6]. This analysis revealed a canyon surrounding each fivefold axis that is wide enough to bind intercellular adhesion molecule-1 (ICAM-1), the cellular receptor, but too narrow to bind an antibody. It was proposed in the canyon hypothesis [7] that this spatial seclusion of a necessarily conserved receptor-binding site might be a general strategy facilitating viral escape from immune surveillance. It was later shown that ICAM-1 does indeed bind into the canyon of HRV16 [8]. However, the structure of foot-and-mouth disease virus (FMDV) suggested that alternative strategies might be used for receptor attachment [5,9], and peptide–antibody complexes for this system [10,11] demonstrate that seclusion of receptor-binding residues is not a general requirement [12], a view supported by the structure of an antibody–HRV14 complex [13].

Alignments of enterovirus sequences show that CAV9 possesses an approximately 15 amino acid insertion at the C terminus of VP1 which contains an arginine-glycine-aspartate (RGD) tripeptide [1], a motif known to interact with integrins [14]. Analysis of CAV9 sequences isolated over a 25 year period show that the RGD motif is conserved but most of the surrounding residues are variable [15], implying that the tripeptide has a functional role. Binding experiments have shown that RGD-containing peptides block CAV9 infectivity in green monkey kidney (GMK) cells [16] and the cellular receptor has been identified as the integrin $\alpha_v\beta_3$ [17], also known as the vitronectin receptor. CAV9 mutants lacking the RGD motif have a small-plaque phenotype in monkey kidney cells, but in human rhabdomyosarcoma (RD) cells infectivity is the same as with RGD-containing viruses [18]. This suggests an alternative receptor-binding site which is evidently more important in RD cells. A recent study on the kinetics of uncoating has confirmed that there are two different entry routes into host cells, only one of which is dependent on the RGD sequence [19].

The virus most similar to CAV9 (based on RNA sequence) for which there is a known three-dimensional structure is coxsackievirus B3 (CBV3) [20]. CBV3 uses two different receptors, coxsackie and adenovirus receptor (CAR) [21] and decay accelerating factor (DAF) [22]. On the basis of the extent of conservation of surface residues, it has been proposed that the canyon and the twofold depression are binding sites for CAR and DAF, respectively [20].

In order to be capable of disassembly and yet maintain stability outside the host, the virus must be able to make a triggered conformational change. In the case of enteroviruses and rhinoviruses, uncoating is believed to occur by the formation of A particles [23], virions with an altered structure that have been observed by electron microscopy. Three features of viral structure have been discussed as potential modulators of uncoating: a hydrophobic pocket, in VP1, under the base of the canyon that can bind so-called pocket factors thus stabilising the capsid [24,25]; a myristoyl group bound to the N terminus of VP4 that may insert into the host membrane [26]; and ions on the fivefold axis that may respond to the change in pH of the endocytotic vesicle and allow extrusion of the RNA through the vertex of the fivefold axis [27]. Although the nature of the events leading to uncoating remains unclear, compounds that bind tightly within the VP1 pocket inhibit uncoating and represent potential therapeutic agents. An example of such a compound is WIN 51711 [28].

Here we report the 2.9 Å resolution structure of CAV9 in complex with WIN 51711. Electron density for the C terminus of VP1 is clear up to six residues prior to the RGD motif, so although we cannot visualise this site its approximate location can be inferred. Several unexpected features are presented here, such as additional WIN molecule-like density at the mouth of the pocket, the first continuous model of the VP1 N terminus of an enterovirus, and ion-like spherical electron densities along the fivefold and threefold axes.

Results and discussion

Overall structure

The data set was 41.1% complete with an overall R merge of 17% (Table 1). The structure was solved by molecular replacement and refined using strict noncrystallographic constraints, see the Materials and methods section. The electron-density maps were of good quality. A sample region of the final $2F_o–F_c$ map for part of VP2 is shown in Figure 1. The final R factor for the model was 16.9%. In light of the excellent ratio of X-ray observations to parameters (373,000 reflections and 6540 atoms), the good stereochemistry of the model (root mean square deviation [rmsd] for bond lengths 0.012 Å), and the satisfactory backbone torsion angles (87.3% of the residues lie in the most favoured region of the Ramachandran plot that the program PROCHECK [29] produced), the model can be considered as essentially refined. The structure of a protomer is shown in Figure 2. The secondary structures, solvent accessibility and sequence conservation between CAV9 and CBVs are summarised in Figure 3.

As the structural analysis suggested some disagreement between the electron-density map and the original amino acid sequence deduced from the CAV9 cDNA clone [1], the capsid protein-coding region of the clone was resequenced. Comparison between the sequences showed eight amino acid differences; these residues were found in VP1 at positions 11 (Arg/Val original/new sequence),

Table 1

Data collection and refinement statistics.

Data collection and processing	
D_{min} (Å)	2.9
Number of crystals	8
Number of images	92
Number of reflections	697,000
Number of unique reflections	290,000
R merge (%)*	17
Completeness (%)†	41
I/σ(I)	4.2
Correlation coefficient (%)‡	88.7
Refinement	
Data range (Å)	20–2.9
Final statistics	
R factor (%)§	16.9
Protein model	6540 Atoms 843 Residues
Solvent	448 Water molecules
Nonprotein atoms	15 (Myristoyl groups) 50 (2 WIN molecules)
Rmsd bond lengths (Å)#	0.012
Rmsd angles (°)#	1.79
Rmsd B (bonded; Å^2)¶	3.7
Rmsd B (angle-related; Å^2)¶	5.4
Mean overall B factor for mainchain atoms (Å^2)	23.8

*$R = 100 \times \Sigma_h \Sigma_j \left| \left| I_{h,\,merged} \right| - \left| I_{h,\,j} \right| \right| / \Sigma_h N \left| I_{h,\,merged} \right|$, where j = 1, …, N for N data sets. †Completeness of the highest resolution shell (3.1–2.9 Å) was 32%. ‡Correlation coefficient = $100 \times \Sigma_h (< F_{obs} > - \left| F_{h,obs} \right|)(< F_{av} > - \left| F_{h,av} \right|) / [\Sigma_h (< F_{obs} > - \left| F_{h,\,obs,} \right|)^2 \times \Sigma_h (< F_{av} > - \left| F_{h,\,av} \right|)^2]^{1/2}$. §$R = 100 \times \Sigma_h \left| \left| F_{h,\,obs} \right| - \left| F_{h,calc} \right| \right| / \Sigma_h \left| F_{h,obs} \right|$. #Root mean square deviation (rmsd) from ideal bond lengths or bond angles. ¶Rmsd of B factors for the bond or angle restraints.

12 (Cys/Val), 13 (Thr/His), 20 (Thr/Ser), 84 (Lys/Asn), 85 (His/Asp) and 142 (Arg/His). In addition, a residue at position 110 of VP2, which was leucine in the database sequence but valine in the original article [1], turned out to be valine in this analysis. The electron density is entirely consistent with the new sequence.

Superimpositions with other picornavirus structures are shown in Figure 4. Table 2 shows quantitatively the structural similarities between CAV9 and some other picornaviruses. Amongst the enteroviruses, CAV9 is most similar to CBV3 and least similar to bovine enterovirus (BEV). Slightly more similar than BEV is HRV14, which belongs to a different genus. The capsid region sequence identities of BEV and HRV14 to CAV9 are 73.1% and 79.5%, respectively, which also questions the classification of BEV. As expected Mengo virus in the cardiovirus genus and FMDV in the aphthovirus genus are the most distant from CAV9.

VP1

VP1 contains 299 residues, of which the first 284 have been built into the map. The β-barrel structure of known picornavirus structures is well conserved with eight β strands (B–I), however, some loop regions adopt distinct conformations (Figure 4a). In particular, the three loops that cluster at the fivefold axis (the BC, DE and HI loops; residues 81–89, 128–140 and 224–231) vary most in structure from those of CBV3. The BC loop has a three-residue insertion in CAV9 relative to CBV3.

The N-terminal 12 amino acids were not present in the phasing model, and were built into the map after two rounds of modelling and refinement. The N terminus forms a finger that points towards the base of the fivefold axis (Figure 4a), in a similar position to the tentative models of poliovirus VP1 N-terminal segments [24], which were given an arbitrary sequence. There are mainchain hydrogen bonds between the VP1 residues 2–6 and the VP4 residues 3–5, characteristic of a parallel β sheet, which may explain why both VP4 and the N terminus of VP1 are found to be externalised in A particles.

The CAV9 electron-density map shows ordered density up to residue 284 of VP1, that is, six residues before the RGD motif and 15 residues before the C terminus of the protein. This implies that, in common with the structure of the RGD loop in FMDV [5], the sequence does not form a single conformation. Residues 282–284 differ from the VP1 C-terminal residues of CBV3, detaching themselves from the outer surface of the virion near the C strand of the VP3 β barrel.

VP2

The β barrel follows the same path as that of other VP2 structures, the largest feature being the 'puff' region made up of the EF loop (residues 129–178). Of the 261 residues of VP2, all but the N-terminal nine residues are present in the model. The N terminus starts on the inner side of the capsid towards the icosahedral threefold axis and finishes exposed to the surface close to the twofold axis. The least conserved area of the structure with respect to CBV3 is the puff, and this region has been implicated in receptor binding in poliovirus [30] (Figure 4b). The puff is made up of two sequential loops, and the second is more exposed on the virus surface. In CAV9 there is a two-residue deletion in the second loop compared to CBV3.

Pro83 is clearly a *cis* proline (Figure 1), although it was assigned as *trans* in the CBV3 structure, which was used for the initial model for molecular replacement. This proline is perfectly conserved among picornaviruses [31], and adopts a *cis* conformation even in HRV14, Mengo virus and FMDV [31,32]. Therefore, we suggest that it is a general feature of picornaviruses. It has been suggested that isomerisation of this proline residue might influence neighbouring structural features, such as the orientation of helix A involved in pentamer–pentamer interactions [31].

VP3

VP3 contains 238 residues, all of which are modelled into the structure (Figure 4c). The conserved β barrel is

Figure 1

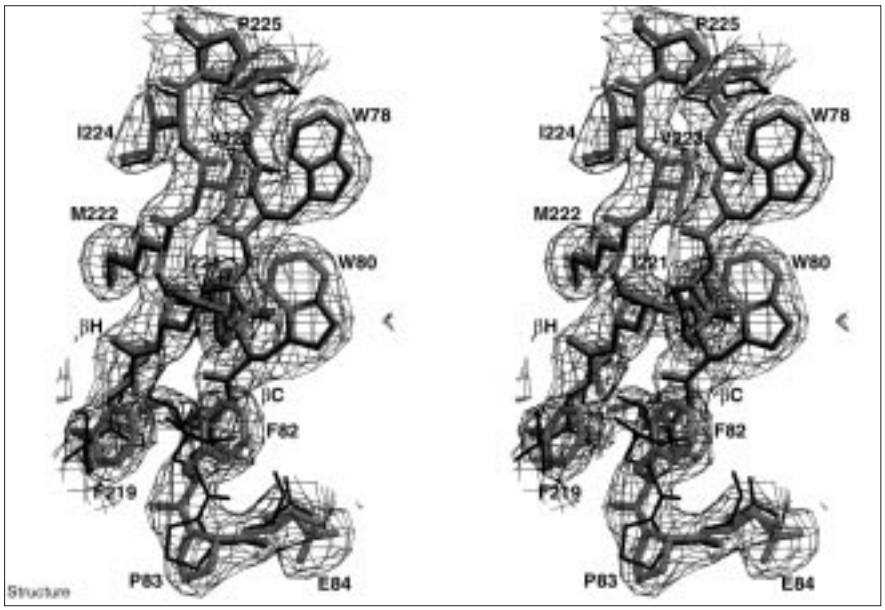

Stereoview of a sample region of the $2F_o–F_c$ map from CAV9 VP2 contoured at 3σ, shown as black mesh with the atoms of CAV9 connected by thick grey rods. The figure was generated using a version of MOLSCRIPT [51] modified by R Esnouf (BOBSCRIPT [52,53]) and Raster3D [54].

relatively compact, and an extended N-terminal tail begins close to the fivefold axis, stacked above the N termini of VP1 and VP4 bringing it closer to the outer surface. The fivefold related N termini form a β cylinder, which is likely to be important in pentamer formation and stability. On the other hand the VP3 C terminus appears on the virus surface. The most prominent surface protrusion is the 'knob' formed by residues 58–69. This loop is also the most variable in structure compared with other picornaviruses.

Figure 2

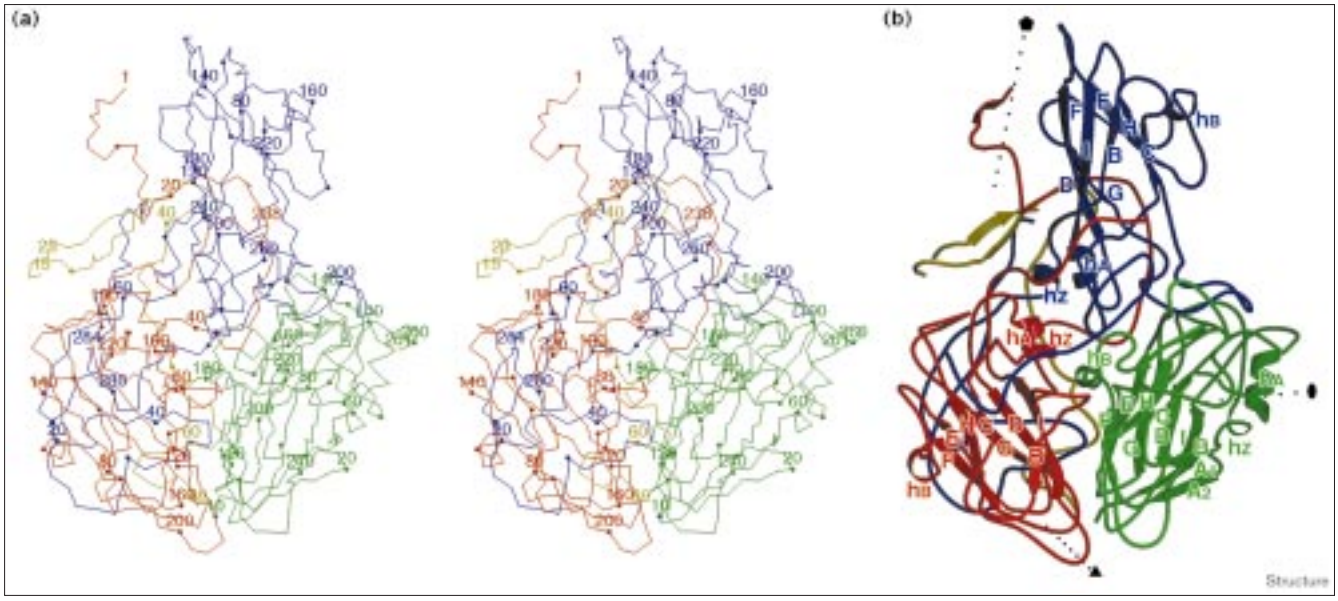

Structure of a CAV9 protomer unit. The different viral proteins are colour-coded: blue, VP1; green, VP2; red, VP3; yellow, VP4. (a) Stereoview Cα trace, dotted every tenth residue and numbered every twentieth residue. (b) Ribbon depiction illustrating the secondary structure elements. Major secondary structure elements are labelled, with β strands BIDG and CHEF forming opposing β sheets and flanking helices prefixed by 'h'. The fivefold, threefold and twofold axes are shown by dotted lines and labelled with a pentagon, a triangle and an oval, respectively. The figure was generated using a version of MOLSCRIPT [51] modified by R Esnouf (BOBSCRIPT [52,53]) and Raster3D [54].

Figure 3

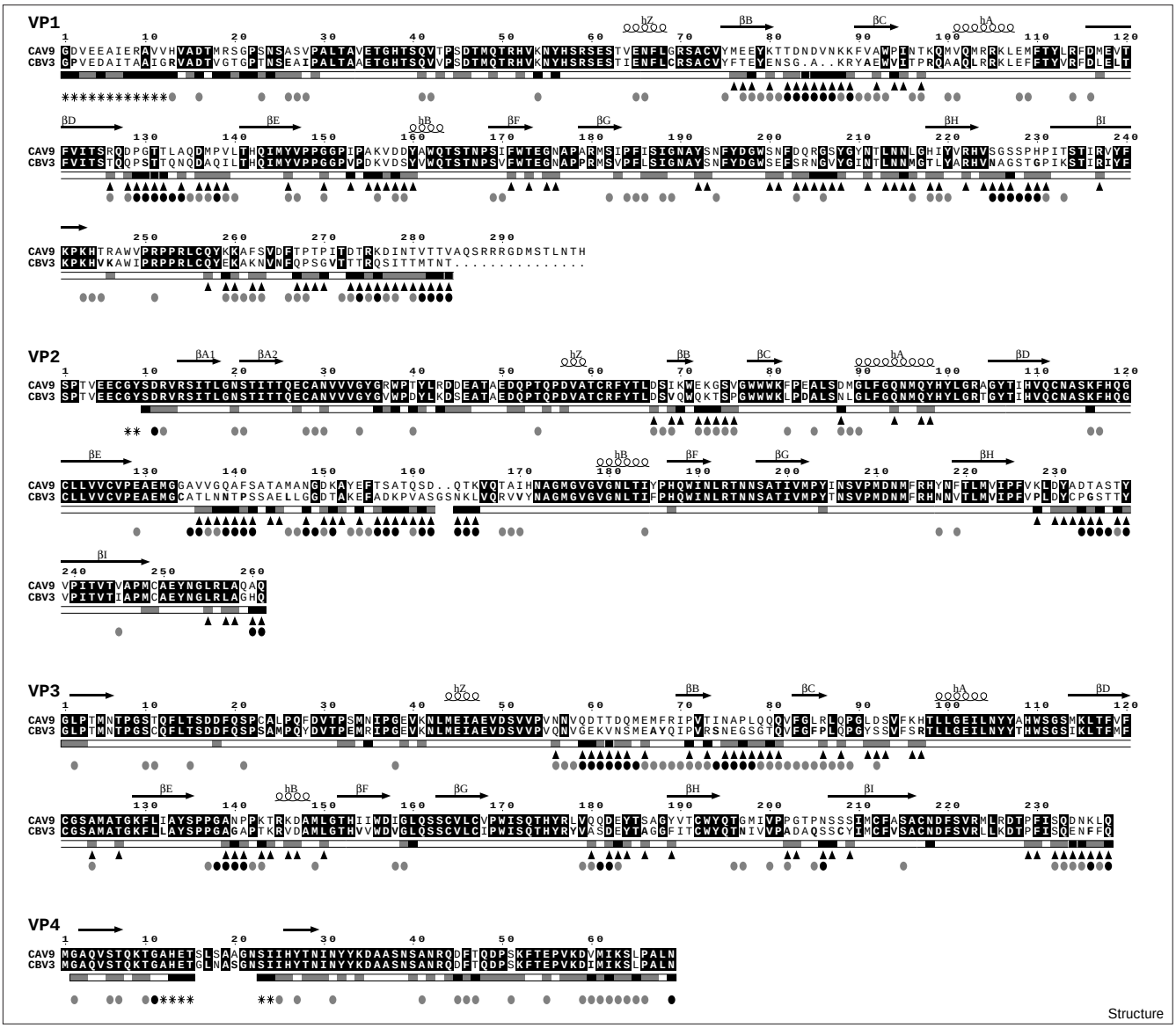

The sequence of the capsid region of CAV9 aligned with that of CBV3. The alignment was made using CLUSTAL-W [55] and corrected by eye and by using structural alignment with SHP [56]. Residues conserved among CAV9, CBV3 and other CBVs are shown boxed with a black background. Helices and strands, assigned manually, are labelled and represented by squiggles and arrows, respectively. Solvent accessibility was calculated by DSSP [57] in the presence of neighbouring symmetry-related protomers, and is shown by the darkness of bars below the sequence; black with a relative accessibility > 40% and grey > 10%. Residues located on the external virion surface are shown by black triangles. The bottom row marks with grey and black ovals those residues for which the Cα distance between CAV9 and CBV3 is larger than 0.5 and 1.0 Å, respectively; asterisks are added where one of the two structures is missing. This figure was produced using the program ESPript [58].

VP4

VP4 is the most conserved of all the viral proteins and lies on the interior of the capsid (Figure 4d). After two rounds of modelling and refinement nearly all the structure could be modelled into the density, with the exception of the loop region from 16–22 corresponding to the most variable sequence. The 69 amino acid chain has little secondary structure, beginning close to the icosahedral fivefold axis and snaking towards the threefold axis. The N-terminal glycine is covalently attached to a myristic acid moiety by an amide linkage, and the myristoyl groups cluster around the fivefold axis underneath the VP3 β cylinder. The carboxylate group of the lipid forms a hydrogen bond with Thr28 of VP4. The C terminus of VP4 is close to the N terminus of VP2, but because the nine residues at the start of VP2 are not visible it is not possible to define the

precise relationship between the two termini which are covalently linked prior to cleavage of VP0, the final step in the maturation of the virion.

Visible RNA

A region of density resembling an RNA nucleotide is seen interacting with the inner surface of the protein shell, making a ring-stacking interaction with Trp38 of VP2. This residue is highly conserved amongst the picornaviruses, and similar density, possibly corresponding to a purine base, is seen in other structures in this position [20,24,32,33].

Surface characteristics and receptor binding

Around each fivefold protrusion there are five distinct depressions ~15 Å deep (Figures 5a–c), rather than a continuous circular canyon. The structure forming a ridge between each depression is composed of the C terminus of VP3, the first loop of the puff of VP2, and residues of C-terminal loop (around residue 260) of VP1. The ridges are curved giving the surface of the pentamer the appearance of a propeller. The depression on the icosahedral twofold axis, also ~15 Å deep, is enclosed by four walls made up of symmetry-related pairs of VP3 and VP2.

In CAV9, the RGD motif (residues 290–292) lies approximately centrally within the 15-residue C-terminal extension of VP1, which is not visible in the structure. Six residues N-terminal to this region, residue 284 can be visualised on the surface of the virus. There is a negatively charged patch close to residue 284 of VP1 (Figure 5b), which may interact with the triple arginine motif which precedes and overlaps the RGD motif. This patch includes Asp182 and Glu183 (VP3) and is adjacent to the drug-binding site located at the centre of the canyon depression. This would enable Asp292 in the RGD motif to contact Arg205 (VP1), a positively charged residue on the structure separating the canyon and twofold depressions. We find continuous weak electron density starting

Figure 4

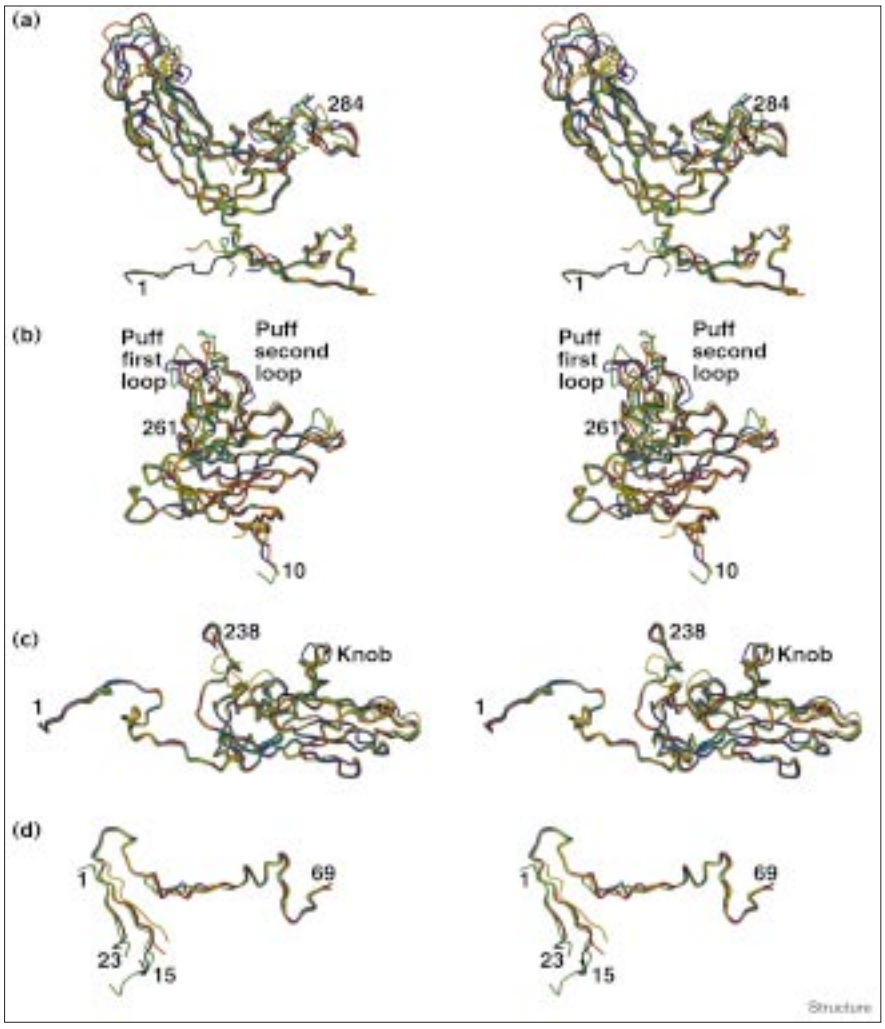

Stereoview superimpositions of the CAV9 structure with those of other picornaviruses. (a) VP1, (b) VP2, (c) VP3 and (d) VP4. The structures are colour-coded: black, CAV9; red, CBV3; blue, type-1 poliovirus; green, HRV14; yellow, BEV. PDB entries used are shown in Table 2, and superimposition was made using SHP [56]. Parts (a), (b) and (c) are oriented so that the closest fivefold axis is vertical and the twofold axis is in the plane. In (d), VP4 proteins are rotated by 90° so that the fivefold axis is perpendicular to the paper. The figure was generated using a version of MOLSCRIPT [51] modified by R Esnouf (BOBSCRIPT [52,53]) and Raster3D [54].

Table 2

Comparison of the structure of CAV9 with those of other picornaviruses.

	PDB entry	Number of equivalent residues	Rms distance of Cα atoms (Å)*	Sequence identity for equivalent residues (%)
CBV3	1cov	794	0.62	75.4
Polio1	2plv	787	0.94	56.0
HRV14	1r08	750	0.85	50.1
BEV	1bev	734	0.98	48.0
Mengo	1mec	592	1.34	29.1
FMDV	1fmd	518	1.33	23.7

*Superimpositions were performed using the program SHP [56]; rms, root mean square.

from above Arg205 (VP1) running along the wall of the canyon depression up to His218 (VP1) (data not shown), but it is too ambiguous to discriminate from solvent or to build a model of the C-terminal segment of VP1.

Thus, the terminal 15 residues of VP1 do not form an integral part of the virus structure, in line with the observed viability of mutants lacking this region [18]. Many of the structurally characterised integrin ligands [5,34,35] present the RGD motif in an exposed mobile loop, and this mobility may be important in ligand binding.

Although the RGD motif is essential for binding to integrins, it is likely, by analogy with better studied integrin–ligand pairs, that attachment will also involve other portions of the virion surface. For example, a site on one FNIII domain of fibronectin synergises with an adjacent domain bearing the RGD to form the integrin-binding site [36]. Figure 5b shows two patches crowded with charged residues: one is located around the fivefold axis and close to the surface above the WIN molecule bound in the pocket, and the other surrounds the icosahedral twofold axes. These charged patches might contribute to integrin binding or could bind another receptor molecule (e.g. in FMDV, another $\alpha_v\beta_3$ binding picornavirus, a highly charged surface patch binds heparin [9]). However, we cannot find any area of particularly intense electrostatic potential (data not shown).

When the structure of CBV3 was determined, it was proposed, on the basis of conservation among CBVs, that the canyon and twofold depressions (Figures 5d–f) were the respective binding sites for CAR and DAF. In the case of CAV9, one receptor has been identified as integrin $\alpha_v\beta_3$, but other receptor(s) have not been characterised and it is unclear whether CAR or DAF could also be receptors for CAV9. Figure 5f shows the contribution to the virion surface made by residues conserved among CBVs, and Figure 5c shows that inclusion of CAV9 into the comparison markedly reduces the conserved surface areas. In CAV9 more residues are replaced on the floor of the canyon depression, especially adjacent to the pocket, than are substituted on the floor of the twofold depression, which might suggest that CAR does not bind to CAV9. The remaining conserved residues are located mainly on the border between the biological protomers, implying that these residues might have a role in the process of virus assembly.

The antiviral compound

All of the rhinoviruses and enteroviruses of known structure possess a hydrophobic pocket under the base of the canyon of VP1, which extends from a pore on the virus surface through the interior of the β barrel until it is closed off by loops of VP1. This pocket is thought to be occupied by a natural lipid pocket factor upon release of the virus from an infected cell. In some structures this pocket factor is present, in others its place has been taken by a single antiviral compound, and in the case of HRV14 the pocket is empty [6,32]. It is thought that a kinetic equilibrium exists between occupied and unoccupied pocket states and that the presence of a pocket factor or drug inhibits uncoating [37]. The inhibition could be caused by prevention of the collapse of the hydrophobic pocket or by blocking the flow of ions into the virus interior by increasing the rigidity of the ion ligands. The release of the pocket factor allows the virus structure to 'breathe', presumably allowing the conformational changes necessary for uncoating to be transmitted to the structure surrounding the fivefold axis. In contrast the aphthovirus and cardiovirus genera of the *Picornaviridae* have no hint of, nor room for, a pocket factor. These viruses presumably have no need for such a factor as they have a different mechanism of uncoating, dissociating via pentamers instead of A particles [38].

CAV9 was propagated, purified and crystallised in the presence of the antiviral compound WIN 51711 (Figure 6), indeed it was not possible to reproducibly obtain crystals otherwise. A WIN 51711 molecule is observed in the CAV9 pocket, with the bulkier 4-oxazolinylphenoxy group at the closed end and the smaller 3-methylisoxazole group tucked into the open end (Figure 6a). From the electron density we cannot rule out the possibility that a fraction of molecules bind in the opposite orientation. The predominant orientation for WIN 51711 is the same as that observed in both HRV14 and type-3 poliovirus [39,40], however, the addition of a single methyl group to the oxazoline ring is sufficient to reverse the orientation in HRV14 [39]. A related but shorter compound (WIN 66393) soaked into CBV3 crystals [20] binds the same way round as for CAV9, with the bulkier double ring in the closed end of the pocket. The dimensions of the pocket are very similar in both the CAV9 and CBV3 structures, the major exception being a threonine at residue 97 (VP1) in CAV9 that interacts with the isoxazole ring in place of a proline in CBV3.

Figure 5

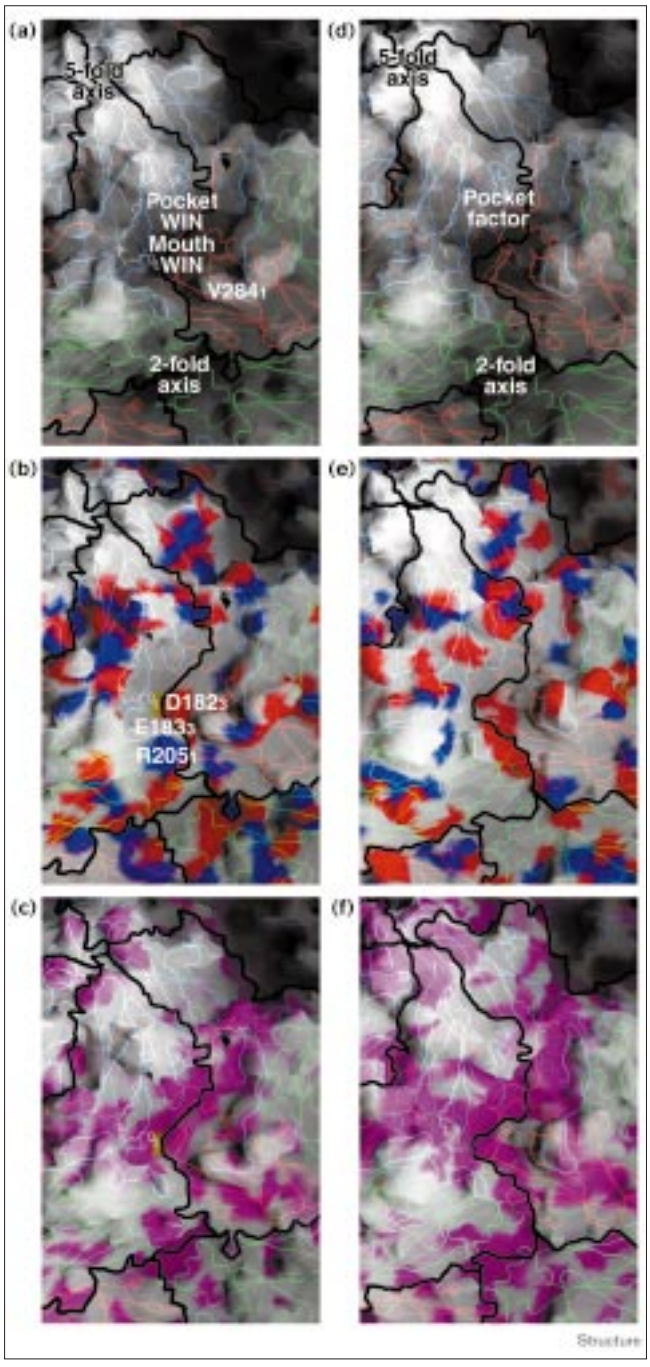

Surface characteristics represented by GRASP [59]. (a–c) CAV9. (d–f) CBV3. Backbone worms are coloured as in Figure 2, and protomer units are bordered in black. WIN compounds or pocket factors are shown as white ball-and-stick models. Parts (a) and (d) are contrasted by radial depth-cueing. Parts (b) and (e) show charged residues: blue, positive; red, negative. Part (c) shows CAV9 residues coloured by the extent of conservation among CAV9 and CBVs; most variable residues are white and strictly conserved residues are shown in magenta. Part (f) shows CBV3 residues coloured by conservation amongst CBVs. The residue number subscript defines the viral protein (e.g. 284_1 is residue 284 of VP1).

It was a surprise to find additional electron density in the vicinity of the entrance to the pocket factor binding site. This density was present in all the electron-density maps calculated and, although at a relatively low level, was consistent in shape between different maps. The density is shown in Figure 6a. We cannot provide a definitive identification of the chemical moiety that this feature represents, however, the general shape does not appear to be consistent with it being polypeptide (C-terminal residues of VP1 might conceivably have attached here, but the distinctive amino acid sequence of this region is not seen). An alternative explanation is that the density might be due to a series of water molecules or possibly dimethylsulphoxide that the WIN compound was dissolved in. Once again we do not feel that these provide a satisfactory explanation for the observed electron density. In fact the density appears to be most satisfactorily explained by a second copy of WIN 51711, blocking the entrance to the hydrophobic pocket. This is the first report for the association of more than one inhibitor for each copy of VP1.

This second or 'mouth' WIN molecule appears to lie head-to-head with respect to the standard or 'pocket' WIN molecule, with the single rings interacting with each other (Figure 6). The double ring of the 'mouth' WIN emerges at the base of the canyon depression slightly exposed to the solvent. This region of the surface appears at first sight to be quite hydrophilic, however, in the presence of this bound moiety the surrounding sidechains are arranged so as to make a binding site with considerable hydrophobic character. There are a total of 11 hydrophobic interactions (including those from an adjacent protomer). Residues contributing to these interactions include Leu216 (VP1), Leu178 (VP3), the aliphatic part of the sidechains of Lys98 (VP1), Asn96 (VP1) and Asn214 (VP1) and the hydrophobic part of the backbone of Tyr192 (VP1). There are also stacking interactions with Tyr210 (VP1) (edge on) and Ile188 (VP1) and polar interactions with polar atoms of the WIN compound. We note additional hydrophobic character within this channel that might be commensurate with the binding of a larger natural pocket factor (the pocket factors observed in rhinoviruses and polioviruses to date have aliphatic chains of 5–16 carbon atoms). This difference might explain some pathological characteristics of this virus such as its preference for cell-specific membrane components, additional to the cellular receptor, as suggested by the observation that different fatty acids have distinct effects on the uncoating of different picornaviruses [41]. An obvious question is whether a larger pocket factor might render the virus particularly conformationally labile in the absence of a pocket factor. Alternatively a longer pocket factor, reaching up closer to the vicinity of the exposed C terminus of VP1, may be better able to 'sense' the binding of the integrin receptor. It is also interesting for the mechanism of uncoating that the mouth WIN is located at the interprotomer interface near the pseudo-threefold axis, a

possible weak point of the capsid. It is usually assumed that removal of the pocket factor primes the capsid for uncoating, alternatively the high concentration of lipid on the cell surface might facilitate lipid exchange with the pocket factor, destabilising the virion.

Ions

There are five spheres of nonprotein density on the fivefold axis that resemble ions (Figure 7b). The two strongest regions of density are ~123 Å and ~112 Å from the centre of the virus. The first is surrounded by the sidechain oxygen atoms of fivefold-related VP3 Thr4 (distance 3.5 Å) and Asn6 (distance 3.7 Å). Chloride has been suggested as a likely candidate for an ion in a similar position in HRV14 [27], although this would be too light to account for the density we observe. The second ion is 4.1 Å from each of the five symmetry-related C9 atoms of the myristylated VP4 N termini. The three weaker regions of density are ~153 Å, ~148 Å and ~139 Å from the centre of the virus and could also be ions, perhaps with lower occupancy. The ions at 153 Å and 148 Å lie next to residues in the DE loop of VP1, but no direct interactions between ion and protein are visible. However, the nearest protein atom to both ions is the sidechain oxygen of Asp136 (VP1) at a distance of 4.1 Å and 5.0 Å, respectively. A putative ion interacting with the DE loop of VP1 has also been found in CBV3, human rhinoviruses and Mengo virus [20,42,4]; in HRV16 (Figure 7c) a zinc ion was putatively assigned at a radius of 152 Å, because of coordination by histidine residues [33,42]. The fivefold ion at 139 Å from the virus centre is 6.3 Å from the mainchain oxygen of Gly175 on the EF loop of VP1.

There is density resembling an ion on the icosahedral threefold axis at ~145 Å radius. The ion is 3.7 Å away from the mainchain oxygen of Pro202 (VP3), in a similar position to an ion found on the threefold axes of CBV3 and HRV14 where interaction is seen with a conserved aspartate residue.

Fivefold axis structure and uncoating

In common with other picornavirus structures [26], CAV9 contains a myristoyl group covalently linked to the N terminus of VP4, with the symmetry-related copies clustering around the fivefold axis (Figure 7a). It has been proposed that during uncoating the RNA and VP4 leave through the fivefold channel [37], that the myristylated VP4 N terminus is involved in interaction with the host cell membrane, and that the previously buried N-terminal region of VP1 becomes exposed [43]. For most enteroviruses and rhinoviruses this region of VP1 is not visible in the structure, however, in CAV9 the N-terminal peptide is resolved and its position, under the N terminus of VP4 on the fivefold axis, is consistent with this hypothesis. The myristoyl group might also stabilise the N-terminal VP3 β barrel and is essential for assembly in at least some picornaviruses [43].

Figure 6

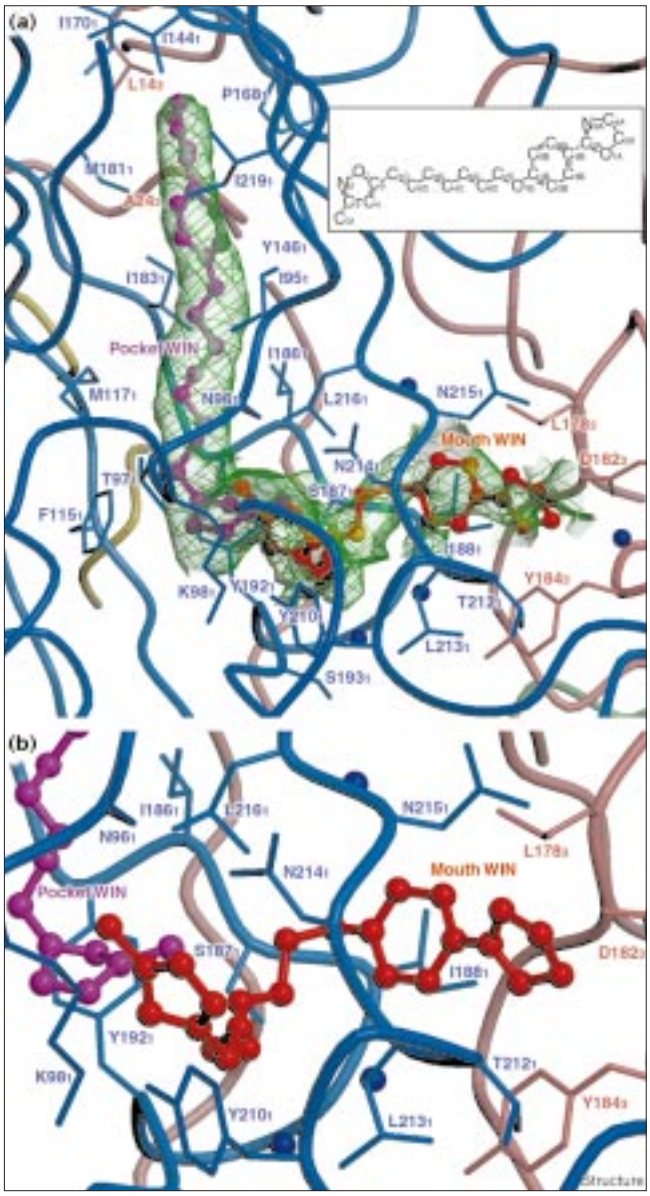

WIN 51711 molecules. (a) The $2F_o–F_c$ maps for the pocket and mouth WIN molecules are contoured at 1σ and 0.5σ, respectively. The WIN compounds are depicted as ball-and-stick models. The protein backbone is represented as a worm, colour-coded as in Figure 2. Residues and water molecules within 4 Å of the WIN molecules are shown as stick models and spheres, respectively. The residue number subscript defines the viral protein (e.g. 98_1 is residue 98 of VP1). The inset shows the chemical structure of WIN 51711. (b) A close-up of the mouth WIN 51711 molecule and surrounding protein. Figure generated using BOBSCRIPT [52,53] and Raster3D [54].

CAV9 provides a continuous model for the VP1 N terminus of an enterovirus (Figure 7b) and as there is also a complete model of the VP1 N terminus for rhinovirus HRV16 (Figure 7c) [33] we can compare the structures at the fivefold axis of the two genera. The VP1 N terminus of CAV9 adopts an extended conformation similar to the

Figure 7

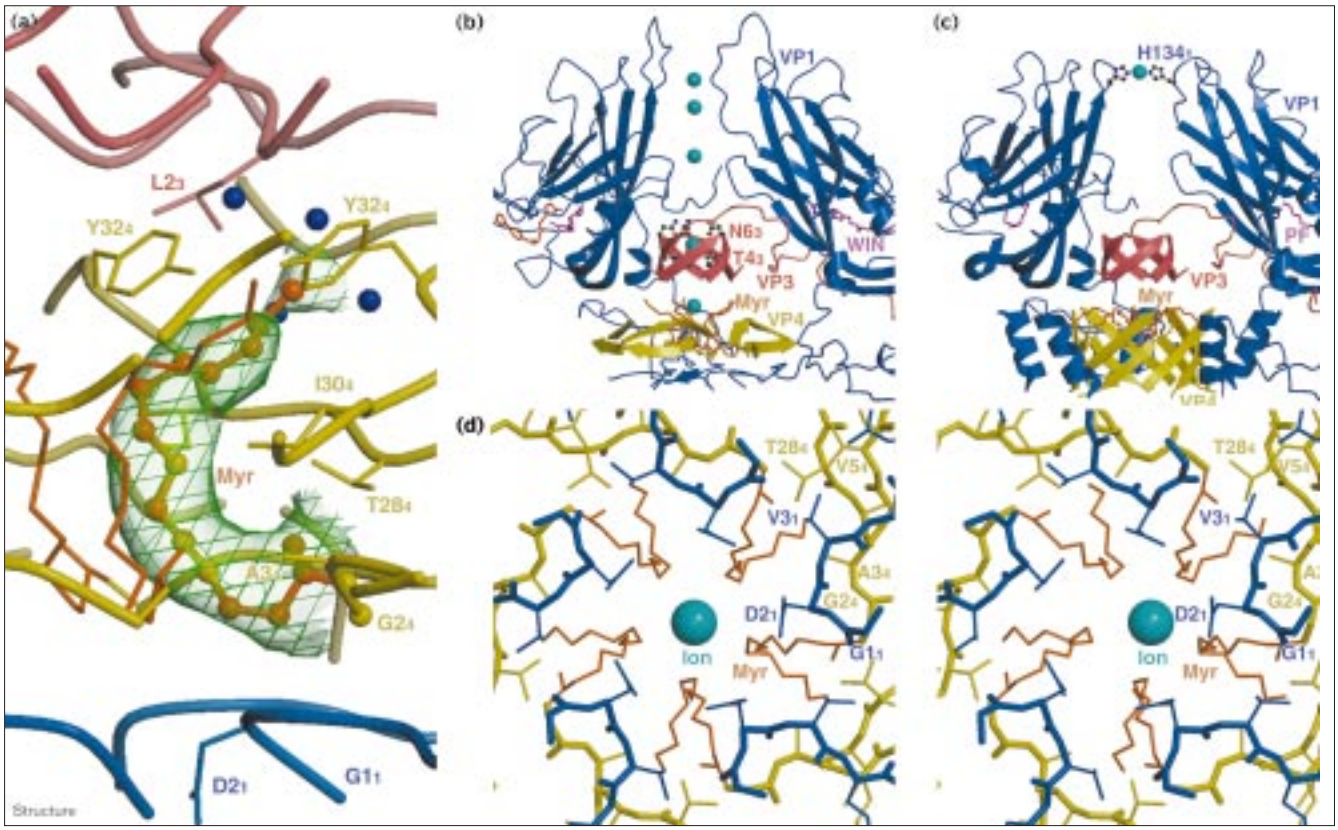

The vicinity of the fivefold axis. (a) A close-up of one myristoyl group, shown as a ball-and-stick model, and a portion of the $2F_o–F_c$ electron-density map contoured at 1σ. Other myristoyl groups are shown as sticks. Protein subunit backbones are depicted as in Figure 6. Residues and water molecules within 4 Å of the myristoyl molecules are shown as stick models and spheres, respectively. Schematic representations of (b) CAV9 and (c) HRV16. The fivefold axis runs vertically through the centre of each figure. Two copies of VP1, WIN compounds and pocket factor (labelled PF), five copies each of VP1, VP3 and VP4 N-terminal strands, one copy of the VP3 N-terminal loop, and fivefold axis related putative ions are shown. Residues close to ions are also shown in ball-and-stick representation with atoms in standard colours. (d) Stereoview detailed structure of CAV9 viewed from the centre of the virion. The backbone and sidechain atoms are shown as thick and thin sticks, respectively. The residue number subscript defines the viral protein (e.g. 28_4 is residue 28 of VP4). Figure generated using BOBSCRIPT [52,53] and Raster3D [54].

unassigned electron density observed for polioviruses [24], which contrasts with the N-terminal helix of HRV16 VP1. The difference in the direction of the two antiparallel β strands from each VP4 N terminus breaks the ten-stranded β barrel of HRV16 (Figure 7c) into five separate β sheets in CAV9 (Figure 7b). So far, all the visible features of this region of the enteroviruses are consistent with those of CAV9, and the features of the other rhinoviruses are consistent with those of HRV16.

However, the fact that the sequences of the first ten residues of VP1 and VP4 are fairly conserved among coxsackieviruses and rhinoviruses makes us wonder what causes the above structural difference. Although a three-residue-long deletion in CAV9 and CBV3 compared with HRVs around residue 12 (VP1) may dictate the extended nature of the coxsackievirus VP1 N terminus, polioviruses have an insertion instead. The helical wheel representation of the VP1 N terminus of CAV9 shows clear amphipathicity (data not shown) as demonstrated for CBV3 and polioviruses [43]; this putative amphipathic helix has been proposed to attach to cell membranes when externalised. This explains the conservation of the VP1 N terminus, but not the observed structural difference at the base of the fivefold axis. The disorder of this structure widely shown among the enteroviruses and rhinoviruses suggests that the above structural difference might not be a strict characteristic of each genus, and these viruses may show considerable conformational heterogeneity even in the resting state. A defining feature of enteroviruses is their greater acid stability and indeed the first seven-residue segment of CAV9 VP1 (Gly-Asp-Val-Glu-Glu-Ala-Ile) is more acidic than that of HRV16 (Asn-Pro-Val-Glu-Arg-Tyr-Val) so that it might require a lower pH to switch it into a helical conformation. However, HRV14 and HRV3 also have acidic VP1 N termini and so this is unlikely to be a general explanation.

It was recently reported that antisera raised against CAV9 reacted to synthetic peptides with the VP3 N-terminal sequence, as well as to VP1 N-terminal peptides [44]. This suggests that the VP3 N terminus might transiently externalise along with the VP1 and VP4 N termini during immunisation. As our structure has confirmed that the CAV9 VP3 N terminus has a location and conformation similar to those of other picornaviruses, this report implies that conformational changes larger than those previously proposed [45] occur and that these might be common to other picornaviruses.

Biological implications

Coxsackievirus A9 (CAV9) is a small icosahedral single-stranded RNA virus that belongs to the genus *Enterovirus* of the family *Picornaviridae*. The capsid enclosing the RNA genome comprises 60 copies of four viral proteins, VP1–4, arranged with pseudo T = 3 symmetry. CAV9 is a clinical pathogen, linked with a variety of illnesses. It is the only CAV so far sequenced that possesses an RGD motif (as part of a 15-residue extension at the C terminus of VP1). Binding to integrin $\alpha_v\beta_3$ has been established, although cell-type-specific, and the virus maintains the use of an alternative unidentified entry route. In the crystal structure of CAV9 reported here, the VP1 C terminus in the vicinity of the RGD motif displays characteristic mobility on the virion outer surface. In addition, sequence comparison in the surface depressions suggests unidentified alternative receptor(s) different from those identified for coxsackie B viruses (CBVs).

Enteroviruses and rhinoviruses have a hydrophobic pocket inside the β barrel of VP1, which is often occupied by fatty-acid-like electron density. This pocket is pharmaceutically important because antiviral drugs (e.g. those named WIN compounds) bind here and inhibit virus uncoating. An unexpected finding for CAV9 is the presence of additional electron density at the mouth of the pocket, consistent with a second WIN molecule, suggesting that a larger natural compound might bind here. This finding has implications for the design of new antiviral compounds and novel strategies for the investigation of uncoating.

The features along the fivefold axis are consistent with the hypothesis that the VP1 N termini and VP4 exit through the fivefold axis, permitting the extrusion of the RNA genome. Differences between the innermost structures of the CAV9 and HRV16 fivefold axes provide a basis for the discussion of uncoating mechanisms.

Materials and methods

Virus purification and crystallisation

The conditions of growth, purification and crystallisation of CAV9 are given in [46], except that 10 μg/ml of WIN 51711 (disoxaril), dispersed in dimethylsulphoxide beforehand, was present during propagation, purification and crystallisation. CAV9 crystals display rhombic plate habit and belong to space group C2 (pseudo I222, see below) with unit-cell dimensions of a = 487.3 Å, b = 358.1 Å, c = 305.7 Å, $\alpha = \gamma = 90°$, $\beta = 128.10°$. There is 30-fold noncrystallographic symmetry as the crystallographic twofold axis coincides with an icosahedral twofold axis.

The capsid-encoding region of the full-length CAV9 cDNA clone (Griggs strain, plaque-purified three times in LLC-Mk_2 cells prior to cloning [1]) was resequenced. Sequencing primers included four sense primers, which annealed to positions 547–567, 1179–1198, 1921–1940 and 2413–2433 of the CAV9 genome, as well as two antisense primers, which annealed to positions 3180–3199 and 3720–3739.

Data collection and reduction

A data set of 41.1% completeness containing 290,000 unique reflections was collected at the Synchrotron Radiation Source (SRS) Daresbury; 33 images were collected on station 7.2 and 59 on station 9.6 with the wavelengths of 1.488 and 0.87 Å, respectively. Statistics on the merged data are shown in Table 1. The exposure times were in the order of 120 s per image. The data were autoindexed and scaled using the HKL package programs DENZO and SCALEPACK [47]. The symmetry of the intensity data indicated that the space group was C2 and the volume of the unit cell was consistent with a crystallographic asymmetric unit comprising half the virus particle.

Structure determination

Measured diffraction intensities were converted to structure-factor amplitudes using the CCP4 program TRUNCATE [48]. In the space group C2 with the virion centre lying on the b axis (the crystallographic twofold axis in the standard definition), determination of the orientation of the virus particle around this axis is sufficient to solve the molecular replacement problem (as the position of the centre of the virion along b is arbitrary). Calculation of a self-rotation function (program X-PLOR [49]) using data from 15–5.5 Å resolution, with a minimum and maximum integration radius of 30 Å and 270 Å, respectively, revealed the orientation of the virion around b. Correlation analysis in reciprocal space using the appropriate portion of the CBV3 virion as a phasing model defined this orientation very precisely, giving a peak at 41.76° rotation from the standard orientation, 39σ above the background level. The initial R factor (see Table 1 for definition) for the orientated CBV3 virus model was 41%, with a correlation coefficient of 43%, and a 30-fold averaged $2F_o–F_c$ map was of good enough quality to build in the CAV9 sequence. Model building was carried out using the interactive graphics program FRODO [50] on an Evans and Sutherland workstation and the structure was refined in X-PLOR [49], using strict 30-fold noncrystallographic symmetry constraints together with a solvent correction. Positional and B-factor refinement was alternated with rebuilding for two rounds, at which point a $2F_o–F_c$ map was calculated and used as the starting point for extensive cycles of 30-fold noncrystallographic averaging. The model was then rebuilt again; WIN 51711, the myristoyl group, more residues of VP1 and VP4 and 448 water molecules were included. Forty cycles of 30-fold averaging were then performed, which converged to give an averaging correlation coefficient of 89% (both WIN compounds were omitted from the phasing model for these calculations). The final R factor for the model was 16.9% and 87% of the residues lie in the most favoured region of the Ramachandran plot. Statistics on the final model are presented in Table 1.

Accession numbers

The coordinates have been deposited with the Brookhaven Protein Data Bank (accession code 1D4M).

Acknowledgements

The authors thank J Grimes and Z Rao for help with data collection, R Bryan and K Measures for computer support and Sterling Winthrop for providing the WIN 51711. G Taylor, R Smallridge and R Westwick are acknowledged for help and support. This work was funded by the MRC, and the Academy of Finland. HH was supported by the Naito Foundation.

References

1. Chang, K.H., Auvinen, P., Hyypiä, T. & Stanway, G. (1989). The nucleotide sequence of coxsackievirus A9; implications for receptor binding and enterovirus classification. *J. Gen. Virol.* 70, 3269-3280.

2. Hyypiä, T. & Stanway, G. (1993). Biology of coxsackie A viruses. *Adv. Virus Res.* 42, 343-373.
3. Hogle, J.M., Chow, M. & Filman, D.J. (1985). Three-dimensional structure of poliovirus at 2.9 Å resolution. *Science* 229, 1358-1365.
4. Luo, M., *et al.*, & Palmenberg, A.C. (1987). The atomic structure of Mengo virus at 3.0 Å resolution. *Science* 235, 182-191.
5. Acharya, R., Fry, E., Stuart, D., Fox, G., Rowlands, D. & Brown, F. (1989). The three-dimensional structure of foot-and-mouth disease virus at 2.9 Å resolution. *Nature* 337, 709-716.
6. Rossmann, M.G., *et al.,* & Vriend, G. (1985). Structure of a human common cold virus and functional relationship to other picornaviruses. *Nature* 317, 145-153.
7. Rossmann, M.G. (1989). The canyon hypothesis. Hiding the host cell receptor attachment site on a viral surface from immune surveillance. *J. Biol. Chem.* 264, 14587-14590.
8. Olson, N.H., *et al.*, & Rossmann, M.G. (1993). Structure of a human rhinovirus complexed with its receptor molecule. *Proc. Natl Acad. Sci. USA* 90, 507-511.
9. Fry, E.E., *et al.*, & Stuart, D.I. (1999). The structure and function of a foot-and-mouth disease virus–oligosaccharide receptor complex. *EMBO J.* 18, 543-554.
10. Verdaguer, N., Mateu, M.G., Andreu, D., Giralt, E., Domingo, E. & Fita, I. (1995). Structure of the major antigenic loop of foot-and-mouth disease virus complexed with a neutralizing antibody: direct involvement of the Arg-Gly-Asp motif in the interaction. *EMBO J.* 14, 1690-1696.
11. Verdaguer, N., *et al.*, & Fita, I. (1998). A similar pattern of interaction for different antibodies with a major antigenic site of foot-and-mouth disease virus: implications for intratypic antigenic variation. *J. Virol.* 72, 739-748.
12. Colman, P.M. (1997). Virus versus antibody. *Structure* 5, 591-593.
13. Smith, T.J., Chase, E.S., Schmidt, T.J., Olson, N.H. & Baker, T.S. (1996). Neutralizing antibody to human rhinovirus 14 penetrates the receptor-binding canyon. *Nature* 383, 350-354.
14. Ruoslahti, E. & Pierschbacher, M.D. (1986). Arg-Gly-Asp: a versatile cell recognition signal. *Cell* 44, 517-518.
15. Chang, K.H., Day, C., Walker, J., Hyypiä, T. & Stanway, G. (1992). The nucleotide sequences of wild-type coxsackievirus A9 strains imply that an RGD motif in VP1 is functionally significant. *J. Gen. Virol.* 73, 621-626.
16. Roivainen, M., Hyypiä, T., Piirainen, L., Kalkkinen, N., Stanway, G. & Hovi, T. (1991). RGD-dependent entry of coxsackievirus A9 into host cells and its bypass after cleavage of VP1 protein by intestinal protease. *J. Virol.* 65, 4735-4740.
17. Roivainen, M., *et al.*, & Hyypiä, T. (1994). Entry of coxsackievirus A9 into host cells: specific interactions with $\alpha_v\beta_3$ integrin, the vitronectin receptor. *Virology* 203, 357-365.
18. Hughes, P.J., Horsnell, C., Hyypiä, T. & Stanway, G. (1995). The coxsackievirus A9 RGD motif is not essential for virus viability. *J. Virol.* 69, 8035-8040.
19. Roivainen, M., Piirainen, L. & Hovi, T. (1996). Efficient RGD-independent entry process of coxsackievirus A9. *Arch. Virol.* 141, 1909-1919.
20. Muckelbauer, J.K., *et al.*, & Rossmann, M.G. (1995). The structure of coxsackievirus B3 at 3.5 Å resolution. *Structure* 3, 653-667.
21. Bergelson, J.M., *et al.*, & Finberg, R.W. (1997). Isolation of a common receptor for coxsackie B viruses and adenoviruses 2 and 5. *Science* 275, 1320-1323.
22. Bergelson, J.M., Mohanty, J.G., Crowell, R.L., St. John, N.F., Lublin, D.M. & Finberg, R.W. (1995). Coxsackievirus B3 adapted to growth in RD cells bind to decay-accelerating factor (CD55). *J. Virol.* 69, 1903-1906.
23. Rueckert, R.R. (1996). Picornaviridae: the viruses and their replication. In *Virology*. (Fields, B.N., Knipe, D.M. & Howley, P.M., eds.), pp. 609-654, Lippincott-Raven Publishers, Philadelphia.
24. Filman, D.J., Syed, R., Chow, M., Macadam, A.J., Minor, P.D. & Hogle, J.M. (1989). Structural factors that control conformational transitions and serotype specificity in type 3 poliovirus. *EMBO J.* 8, 1567-1579.
25. Lewis, J.K., Bothner, B., Smith, T.J. & Siuzdak, G. (1998). Antiviral agent blocks breathing of the common cold virus. *Proc. Natl Acad. Sci. USA* 95, 6774-6778.
26. Chow, M., Newman, J.F.E., Filman, D., Hogle, J.M., Rowlands, D.J. & Brown, F. (1987). Myristylation of picornavirus capsid protein VP4 and its structural significance. *Nature* 327, 482-486.
27. Kalko, S.G., Cachau, R.E. & Silva, A.M. (1992). Ion channels in icosahedral virus: a comparative analysis of the structures and binding sites at their fivefold axes. *Biophys. J.* 63, 1133-1145.
28. Smith, T.J., *et al.*, & Otto, M.J. (1986). The site of attachment in human rhinovirus 14 for antiviral agents that inhibit uncoating. *Science* 19, 1286-1293.
29. Laskowski, R.A., MacArthur, M.W., Moss, D.S. & Thornton, J.M. (1993). PROCHECK: a program to check the stereochemical quality of protein structures. *J. Appl. Cryst.* 26, 283-291.
30. Minor, P.D., Ferguson, M., Evans, D.M.A., Arnold, J.W. & Icenogle, J.P. (1986). Antigenic structure of polioviruses of serotypes 1, 2 and 3. *J. Gen. Virol.* 67, 1283-1291.
31. Krishnaswamy, S. & Rossmann, M.G. (1990). Structural refinement and analysis of Mengo virus. *J. Mol. Biol.* 211, 803-844.
32. Arnold, E. & Rossmann, M.G. (1990). Analysis of the structure of a common cold virus, human rhinovirus 14, refined at a resolution of 3.0 Å. *J. Mol. Biol.* 211, 763-801.
33. Hadfield, A.T., *et al.*, & Rossmann, M.G. (1997). The refined structure of human rhinovirus 16 at 2.15 Å resolution: implications for the viral life cycle. *Structure* 5, 427-441.
34. Adler, M., Lazarus, R.A., Dennis, M.S. & Wagner, G. (1991). Solution structure of kistrin, a potent platelet aggregation inhibitor and GP IIb-IIIa antagonist. *Science* 253, 445-448.
35. Main, A.L., Harvey, T.S., Baron, M., Boyd, J. & Campbell, I.D. (1992). The three-dimensional structure of the tenth type III module of fibronectin: an insight into RGD-mediated interactions. *Cell* 71, 671-678.
36. Leahy, D.J., Aukhil, I. & Erickson, H.P. (1996). 2.0 Å Crystal structure of a four-domain segment of human fibronectin encompassing the RGD loop and synergy region. *Cell* 84, 155-164.
37. Giranda, V.L., *et al.*, & Rueckert, R.R. (1992). Acid-induced structural changes in human rhinovirus 14: possible role in uncoating. *Proc. Natl Acad. Sci. USA* 89, 10213-10217.
38. Fry, E., *et al.*, & Stuart, D. (1992). Molecular studies on the structure of foot and mouth disease virus. In *Protein Engineering.* (Goodenough, P., ed.), pp. 71-80, CPL Press, Berkshire, UK.
39. Badger, J., *et al.*, & Heinz, B.A. (1988). Structural analysis of a series of antiviral agents complexed with human rhinovirus 14. *Proc. Natl Acad. Sci. USA* 85, 3304-3308.
40. Grant, R.A., Hiremath, C.N., Filman, D.J., Syed, R., Andries, K. & Hogle, J.M. (1994). Structures of poliovirus complexes with anti-viral drugs: implications for viral stability and drug design. *Curr. Biol.* 4, 784-797.
41. Smyth, M., Tate, J., Hoey, E., Lyons, C., Martin, S. & Stuart, D. (1995). Implications for viral uncoating from the structure of bovine enterovirus. *Nat. Struct. Biol.* 2, 224-231.
42. Zhao, R., Hadfield, A.T., Kremer, M.J. & Rossmann, M.G. (1997). Cations in human rhinoviruses. *Virology* 227, 13-23.
43. Fricks, C.E. & Hogle, J.M. (1990). Cell-induced conformational change in poliovirus: externalization of the amino terminus of VP1 is responsible for liposome binding. *J. Virol.* 64, 1934-1945.
44. Pulli, T., Lankinen, H., Roivainen, M. & Hyypiä, T. (1998). Antigenic sites of coxsackievirus A9. *Virology* 240, 202-212.
45. Chow, M., Basavappa, R. & Hogle, J.M. (1997). The role of conformational transitions in poliovirus pathogenesis. In *Structural Biology of Viruses*. (Chiu, W., Burnett, R.M. & Garcea, R.L., eds), pp. 157-186, University Oxford Press, New York, NY.
46. Smyth, M., Hall, J., Fry, E., Stuart, D., Stanway, G. & Hyypiä, T. (1993). Preliminary crystallographic analysis of coxsackievirus A9. *J. Mol. Biol.* 230, 667-669.
47. Otwinowski, Z. & Minor, W. (1997). Processing of X-ray diffraction data collected in oscillation mode. *Methods Enzymol.* 276, 307-326.
48. French, S. & Wilson, K. (1978). On the treatment of negative intensity observations. *Acta Crystallogr. A* 34, 517-525.
49. Brünger, A.T. (1992). *X-PLOR Version 3.1: A system for X-ray Crystallography and NMR.* Yale University Press, New Haven, CT.
50. Jones, T.A. (1985). Interactive computer graphics: FRODO. *Methods Enzymol.* 115, 157-171.
51. Kraulis, P.J. (1991). MOLSCRIPT: a program to produce both detailed and schematic plots of protein structures. *J. App. Crystallogr.* 24, 946-950.
52. Esnouf, R.M. (1997). An extensively modified version of MolScript which includes greatly enhanced colouring capacities. *J. Mol. Graph.* 15, 133-138.
53. Esnouf, R.M. (1999). Further additions to MolScript version 1.4, including reading and contouring of electron-density maps. *Acta Crystallogr. D* 55, 938-940.
54. Merrit, E.A. & Murphy, M.E.P. (1994). Raster3D version 2.0. A program for photorealistic molecular graphics. *Acta Crystallogr. D* 50, 869-873.
55. Thompson, J.D., Higgins, D.G. & Gibson, T.J. (1994). Clustal W: improving the sensitivity of progressive multiple sequence alignment through sequence weighting, position-specific gap penalties and weight matrix choice. *Nucleic Acids Res.* 22, 4673-3680.
56. Stuart, D.I., Levine, M., Muirhead, H. & Stammers, D.K. (1979). Crystal structure of cat muscle pyruvate kinase at a resolution of 2.6 Å. *J. Mol. Biol.* 134, 109-142.
57. Kabsch, W. & Sander, C. (1983). Dictionary of protein secondary structure: pattern recognition of hydrogen-bonded and geometrical features. *Biopolymers* 22, 2577-2637.
58. Gouet, P., Courcelle, E., Stuart, D. & Métoz, F. (1999). ESPript: multiple sequence alignments in Postscript. *Bioinformatics* 15, 305-308.
59. Nicholls, A., Sharp, K.A. & Honig, B. (1991). Protein folding and association: insights from the interfacial and thermodynamic properties of hydrocarbons. *Proteins* 11, 281-296.